JACS
JOURNAL OF THE AMERICAN CHEMICAL SOCIETY

ARTICLE

pubs.acs.org/JACS

Shaken, Not Stirred: Collapsing a Peptoid Monolayer To Produce Free-Floating, Stable Nanosheets

Babak Sanii, Romas Kudirka, Andrew Cho, Neeraja Venkateswaran, Gloria K. Olivier, Alexander M. Olson, Helen Tran, R. Marika Harada, Li Tan, and Ronald N. Zuckermann*

The Molecular Foundry, Lawrence Berkeley National Laboratory, 1 Cyclotron Road, Berkeley, California 94720, United States

Supporting Information

ABSTRACT: Two-dimensional nanomaterials play a critical role in biology (e.g., lipid bilayers) and electronics (e.g., graphene) but are difficult to directly synthesize with a high level of precision. Peptoid nanosheet bilayers are a versatile synthetic platform for constructing multifunctional, precisely ordered two-dimensional nanostructures. Here we show that nanosheet formation occurs through an unusual monolayer intermediate at the air−water interface. Lateral compression of a self-assembled peptoid monolayer beyond a critical collapse pressure results in the irreversible production of nanosheets. An unusual thermodynamic cycle is employed on a preparative scale, where mechanical energy is used to buckle an intermediate monolayer into a more stable nanosheet. Detailed physical studies of the monolayer-compression mechanism revealed a simple preparative technique to produce nanosheets in 95% overall yield by cyclical monolayer compressions in a rotating closed vial. Compression of monolayers into stable, free-floating products may be a general and preparative approach to access 2D nanomaterials.

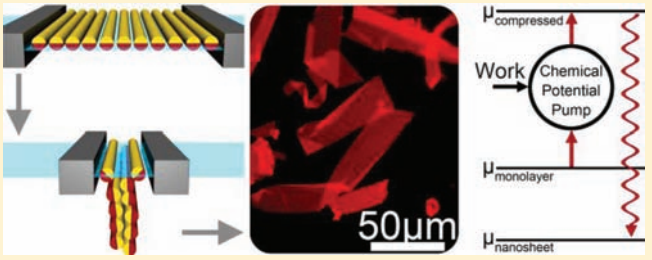

INTRODUCTION

The ability to design and synthesize polymers with structural precision and chemical diversity that rivals natural proteins promises a new class of nanostructured materials with an unprecedented combination of stability and sophisticated function.[1,2] This capability is being realized in a versatile class of synthetic polymers called peptoids. Peptoids are *N*-substituted glycine polymers that are synthesized with monomeric accuracy,[3] drawing from a dictionary of building blocks that is vastly more diverse than those available to peptides. They can bind to biological molecules with high potency and specificity[4] and can fold into protein-like structures,[5] while maintaining resistance to proteolysis.[6] Like peptides, their sequence specificity can encode their structure and function.[7] In an effort to design protein-mimetic peptoid sequences that fold into defined nanostructures, our laboratory has focused on the hierarchical assembly of secondary structural units−helices[5,8] and sheets[7,9]−that are analogous to those found in proteins.

We recently designed specific polypeptoid sequences that assemble into highly ordered supramolecular bilayer nanosheets, with macroscopic lateral dimensions and nanoscopic thickness[7,9] (Figure 1A−C). These nanosheets are particularly interesting, as they serve as a versatile platform for constructing multifunctional, precisely ordered two-dimensional nanostructures.[10−13] Furthermore, peptoid nanosheets are extremely stable and maintain their structure even in the absence of water. Precision control of their molecular structure enables potential applications in a variety of areas, such as platforms for sensing, templating growth, and filtering and as protein mimetics capable of both molecular recognition and catalysis.

The potential broad utility and fascinating structure of these peptoid nanosheets prompted us to scale up their production. Previously we assumed nanosheets form by a solution-phase nucleation-and-growth mechanism,[7,9] but in scaling up their production we discovered puzzling inconsistencies in their preparation. The preparative scale-up of nanomaterials is in fact often not straightforward.[14,15] Here, nanosheets are produced at micromolar peptoid concentrations under physiological conditions when the containing vial is shaken, but not when it is gently stirred. Similarly, no nanosheets are observed without agitation, even after sitting for weeks. These qualitative observations (see the Supporting Information (SI) for a qualitative summary) implicate the role of a dynamic air−water interface in the production of macroscopic nanosheets. This suggests that the efficient production of nanosheets on a large scale requires preparative techniques that provide control over key intermediates that form at the air−water interface.

We report here the quantitative study of an unusual self-assembly mechanism that relies on the formation, compression, and collapse of a peptoid monolayer at the air−water interface (Figure 1D). Unlike most monolayer compression studies, here

Received: July 4, 2011
Published: September 22, 2011

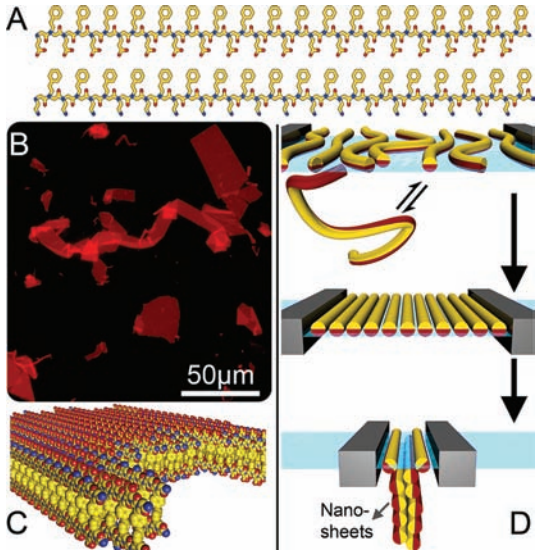

Figure 1. (A) Chemical structure of nanosheet-forming peptoids: a negatively charged amphiphilic peptoid, $(Nce-Npe)_{18}$, and a positively charged amphiphilic peptoid, $(Nae-Npe)_{18}$. Atomic color scheme: carbon, yellow; nitrogen, blue; oxygen, red. (B) Fluorescence microscope image of nanosheets (some overlapped and folded) formed by manually shaking a vial, labeled with hydrophobically active Nile Red dye (2 μM) and deposited on a 1% agarose substrate. (C) Nanosheet model representing the chain organization (far from the edges) of $(Nae-Npe)_{18}$ and $(Nce-Npe)_{18}$. The drawing depicts a bilayer structure with a buried hydrophobic core and is consistent with the AFM-measured thickness and the lateral close-packing of strands suggested by XRD and electron microscopy.[9] Registry between adjacent chains is likely variable.[7] (D) Schematic of the proposed mechanism of nanosheet formation through surface compressions. Peptoids are depicted as rod-like amphiphiles with a hydrophobic half (yellow) and a polar half (red). (Top) Amphiphilic peptoids self-assemble at the air−water interface and are in equilibrium with disordered (or partially ordered) strands in solution. (Middle) Compression increases surface pressure, resulting in closer packing of the chains. (Bottom) The compressed monolayer collapses, producing nanosheets in the subphase.

the product nanosheet provides a deep thermodynamic sink. Thus, we show that nanosheet formation is irreversible, and we describe a repeatable production cycle that converts mechanical energy into highly stable nanosheets, resulting in very high overall yields of nanosheets. The monolayer compression mechanism is critical to the scalable production and engineering of peptoid nanosheets and has implications for the assembly of broad classes of 2D materials assisted by organization of amphiphiles at the air−water interface.[16]

RESULTS AND DISCUSSION

Nanosheet Formation by Vial Rotation. Of the family of peptoid sequences that form nanosheets[7,9] (over 10 identified so far), here we primarily consider a well-characterized pair that form 3 nm thick nanosheets when combined (Figure 1C). These sequences are 36 monomers long and are constructed from only three different monomers: an aromatic, hydrophobic monomer (*N*-(2-phenylethyl)glycine, Npe), and two ionic monomers [*N*-(2-aminoethyl)glycine (Nae) and *N*-(2-carboxyethyl)glycine (Nce)]. They are polymers with a periodic two-fold sequence amphiphilicity, a motif that is known to promote β structure in polypeptides.[17] The oppositely charged strands $(Nae-Npe)_{18}$ and $(Nce-Npe)_{18}$ (Figure 1A) attract each other through both hydrophobic and electrostatic interactions and form free-floating nanosheets under dilute aqueous conditions. These nanosheets have macroscopic lateral dimensions (up to mm), nanoscale thicknesses (3 nm), and a highly organized, close-packed internal structure (4.5 Å strand−strand spacing).[9] Shaking a partially filled vial of these peptoids (see Experimental Section for solution specifics) produces nanosheets as shown in Figure 1B (see SI for a movie of free-floating nanosheets).

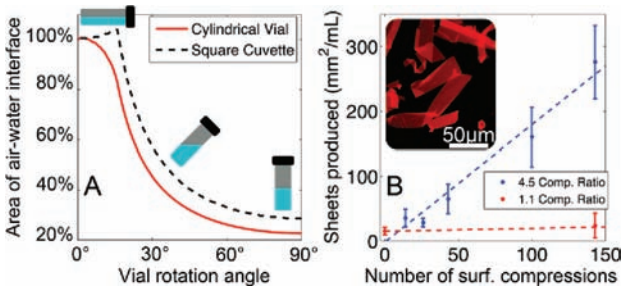

Figure 2. (A) Area of the air−water interface of a half-full container as it is rotated from horizontal to vertical. Analysis shown represents a cylindrical vial (red solid line, 1 cm diameter × 3.5 cm height) and a square cuvette (black dashed line, 1 × 1 × 3.5 cm). (B) Measured area of nanosheets present per unit volume of bulk solution, as a function of number of compressions of the solution in a cylindrical vial (1 cm diameter, 3.5 cm height), with a 450 s wait time between compressions. Blue line corresponds to a full 85° rotation of the vial (compression ratio of 4.5); red line corresponds to a 25° rotation of the vial to vertical (compression ratio of 1.1). A linear fit of the full rotation indicates that 0.9 mm^2/mL of macroscopic sheet material is produced per compression. Inset: Fluorescence image of sheets produced by such surface compressions with rotated vials (labeled with Nile Red dye (2 μM) and deposited on a 1% agarose substrate).

Shaking a vial induces several simultaneous and chaotic mechanical events to occur. These events include shearing, mixing, and interfacial expansion/contraction. However, nanosheets were not produced when the solution was gently stirred (which produces significant shear and minimal surface compression), nor were they produced when the solution was allowed to sit without mixing. We thus hypothesized that expansion and contraction of the air−water interface is the primary determinant for the production of laterally macroscopic nanosheets.

We require a reproducible, preparative technique to directly compare production conditions and structural analogues. We were able to isolate whether expansion and contraction of the air−water interface was responsible for sheet formation with a simple preparative method where a vial is gently rolled end-over-end[18,19] (Figure 2A). A glass vial that is partially filled with peptoid solution is sealed and slowly rotated 85° from vertical, allowing the air−water interface to expand along the length of the vial. After an appropriate pause, the vial is rotated back to vertical, resulting in a compression of the exposed surface by a factor of ~4, depending on the exact vial geometry and sample volume. For example, ignoring the meniscus effect, a half-full 1 × 1 × 4 cm rectangular vial lying on its side has an exposed interface of 4 cm^2. However, when rotated to an upright position, the exposed interface shrinks to 1 cm^2, applying a 4:1 compression ratio during the rotation. The reduction in surface area is not

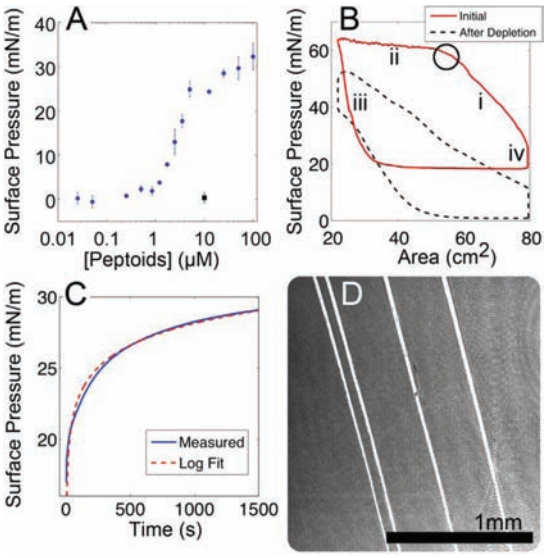

Figure 3. (A) Surface pressure as a function of the concentration of the peptoid solution. Measurements were taken by the capillary rise method within 2 min of the interface forming. Black square indicates the surface pressure of a 10 μM peptoid solution 4 days after the available material in the subphase is depleted by over 700 compressions (see Figure 4D for depletion isotherms). (B) A typical Langmuir trough isotherm of 10 μM peptoid solution compressed at 100 cm^2/min with a wait time of 450 s between compressions. Labels indicate the four regions described in the text (i, compression; ii, collapse; iii, expansion; iv, adsorption) and the collapse point (black circle). The dashed black line indicates the isotherm after subphase material is essentially depleted by over 700 compressions. (C) Surface pressure of a 10 μM peptoid solution as a function of time since the interface monolayer was removed by aspiration. The dashed red line indicates a log fit. (D) BAM image of the surface of a 3 μM peptoid solution after compression beyond the collapse point. Image was transformed such that the pixel dimensions are square and high-pass filtered to remove uneven illumination for clarity.

linear with time given a constant rotation velocity, but the compression rate can be controlled by modulating the angular velocity (see Figure 2A and SI for analysis and modeling). We therefore developed a microcontroller-based, variable-speed vial-rotating apparatus (see SI for instrument design) that follows an angular velocity trajectory that mimics linear compression of the air−water interface and can pause for specific time intervals between compressions.

Using this preparative surface-compressing vial rotation method with an equimolar mixture of the sheet-forming peptoids $(Nae-Npe)_{18}$ and $(Nce-Npe)_{18}$ (see Experimental Section), we found that nanosheets emerge in the subphase without the need for shaking. Qualitatively, as seen in Figures 1B and 2B (inset, also see SI for a movie of free-floating nanosheets made by surface compressions), the average size of the macroscopic sheets was significantly larger when sheets were produced from vial rotation vs vial shaking, and the edges appeared cleaner and more distinct. However, it is difficult to discern whether this is due to the formation mechanism or due to the effects of agitation on the sheet after it formed, as sheets break. The frequently observed straight-edge feature of the nanosheets could be a consequence of fracture and edge-reorganization along grain boundaries. Sheets prepared by vial rotation or by shaking have indistinguishable molecular structural characteristics, as evidenced by atomic force microscopy (AFM)-measured thicknesses and X-ray diffraction (XRD, see SI).

If stable sheets are produced from surface compressions, we would expect a monotonically increasing relationship between the number of vial rotations and the amount of sheets in solution. We tracked the yield of peptoid nanosheets in solution by imaging a fixed volume of them by fluorescence microscopy and determining their cumulative area using custom sheet-counting analysis software (see SI). Sheet area per unit volume increased linearly with the number of compressions (Figure 2B), indicating that nanosheets are directly produced from surface compressions. Each data point represents an independent vial of solution, stored adjacent to the vial-rotator when not undergoing surface compressions. All the vials were mixed by gentle pipet aspiration at the start of the experiment, and final measurements occurred after all the samples had undergone their compressions. With this approach, sheets formed from spurious changes to the air−water interface (e.g., room vibrations) are accounted for. As all of the vials were mixed and measured at approximately the same time, yet produced vastly different amounts of sheets, we can eliminate the likelihood that nanosheets form spontaneously in the bulk or from a static interface over time.

Collapse of a Peptoid Monolayer. In order to explore the behavior of these peptoids at the air−water interface, we determined the relationship between their mixed concentration in solution and the ensuing (within 2 min) surface pressure, using a capillary rise method.[20,21] Like many amphiphiles, the surface pressure as a function of mixed peptoid concentration is sigmoidal (Figure 3A). It does not rise appreciably until the peptoid concentration is greater than 0.1 μM (in each peptoid). At low peptoid concentrations (<1 μM), sheet production is not observed (see SI). Concentrations greater than 10 μM do not significantly increase the surface pressure, indicating that 10 μM approaches a critical aggregation concentration. Concentrations above 50 μM visually appear cloudy upon initial mixing, consistent with an aggregation threshold. Thus, within the concentration window of 0.1−10 μM, we expect a monolayer of peptoids at the air−water interface, with minimal macroscopic aggregates in the subphase.

The physical properties of the peptoid monolayer formed in the 1−10 μM concentration window were analyzed with a Langmuir trough. In a departure from traditional Langmuir trough experiments, here the molecules of interest are soluble and present in the subphase at significant concentrations. When peptoids are removed from the air−water interface, the monolayer spontaneously repopulates from the excess reservoir of free peptoids in the subphase. We note that, compared to vial rotation, a symmetric Langmuir trough is an imperfect preparative technique, as every expansion between the barriers causes a corresponding compression of the surface on the other side of the barriers. Additionally, it is more susceptible to contamination and evaporation, and not conveniently scalable in size. Nonetheless, the ability to measure the surface pressure with a Wilhemy plate during compressions reveals interesting characteristics that provide key insights into the nanosheet formation mechanism.

Mechanically compressing the air−water interface in the Langmuir trough while measuring the surface pressure reveals an isotherm with four distinct regions (i−iv, Figure 3B). The surface pressure increases linearly with compression (i), but at a distinct point the slope reduces significantly to enter another linear region (ii). We refer to the point where the slope changes between (i) and (ii) as the "collapse pressure", which for the

standard sheet-forming solution of 10 μM per peptoid at room temperature (see Experimental Section) is 54.5 mN/m at the center of the trough. Upon expansion (iii) the surface pressure quickly drops, and the isotherm exhibits a large hysteresis. When the trough is open and stationary (iv), the surface pressure continues to increase logarithmically with time (Figure 3C), indicating the gradual re-formation of the monolayer by adsorption of free peptoids in the subphase.

Compression cycles below the collapse pressure do not produce macroscopic sheets. While this effect is also seen on the symmetric Langmuir trough, for the reasons outlined above it is preferable to track sheet production with a rotating vial. We rotated vials 143 times with a 450 s wait time between compressions, through a 25° angle range that corresponds to a compression ratio of 1.1, which is less than the 1.5 compression ratio required to reach the collapse pressure. Analysis of the subphase yielded a negligible amount of nanosheets compared to the identical number of full compressions with a 4.6:1 compression ratio (see Figure 2B).

The collapse is a large-scale mechanical failure, as seen in images of the surface from a Brewster angle microscope (BAM)[22] (see Figure 3D). These events manifest as discontinuities in the surface pressure isotherm and are so dramatic that one can observe them by eye as ripples extending across the air−water interface. Small compressions to surface pressures below the collapse pressure are largely reversible and exhibit little surface pressure hysteresis, whereas compressions beyond collapse exhibit significant hysteresis, implying irreversible changes to the monolayer (see Figure 4A). Thus, compressions beyond collapse coincide with isotherm hysteresis, mechanical failure, and the emergence of nanosheets in the subphase.

Peptoid Nanosheet Production Cycle. The sheet production cycle can be broken down into four distinct regions of the monolayer compression isotherm: compression, collapse, expansion, and adsorption (Figure 3B). In the compression region (i) the surface monolayer behaves elastically, with little hysteresis. At the collapse pressure the surface relieves the excess surface pressure by buckling at multiple locations. Continued compression continues to collapse (ii) the monolayer. Hysteresis in the isotherm upon expansion (iii) indicates that the monolayer was irreversibly altered, consistent with losing material into the bulk. Pausing with an open trough allows the re-adsorbtion (iv) of the peptoids as a monolayer, increasing the surface pressure. Subsequent compression cycles produce comparable isotherms and linearly increase the population of macroscopic sheets in the subphase (until depletion of available peptoid material becomes a significant factor).

An important parameter for producing nanosheets by surface compressions is the wait time between compressions (Figure 3B, iv). If the monolayer is not given sufficient time to re-form/re-organize, then a significantly greater compression is required to reach the collapse pressure (Figure 4B). After a compression cycle (or after surface aspiration), re-forming a peptoid monolayer at the air−water interface is gradual (Figure 3C). The lengthy recovery time may be due to slow adsorption or ongoing reorganization, in a manner reminiscent of amyloid reorganization at the air−water interface.[23] The adsorption continues until the system achieves a distinct "equilibrium monolayer pressure", where the rate of peptoid display equals the rate of dissolution into the subphase. We determine the equilibrium pressure by measuring the change in trough area required to maintain a fixed pressure. When set

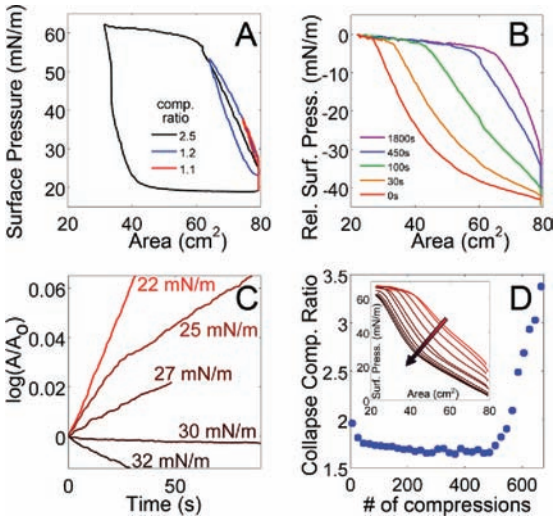

Figure 4. (A) Three isotherms of 10 μM peptoid solution to different compression ratios, indicating significant hysteresis after reaching the collapse pressure. (B) 100 cm^2/min compression isotherms of a 10 μM peptoid solution as a function of the wait time between compressions. Isotherms are normalized to the surface pressure of collapse to account for evaporation drift. (C) Trough areas required to maintain fixed surface pressures over time. Fixing the surface pressure at 30 mN/m requires minimal adjustment of the trough area over time, indicating that this is approximately the equilibrium monolayer surface pressure for a 10 μM peptoid solution. (D) Compression ratio required to achieve monolayer collapse with the 10 μM peptoid solution as a function of the number of compressions performed (every 20th shown). Inset: Compression isotherms as the subphase is depleted of available peptoids. Traces indicate every 20th compression, starting with the 401st compression. Compressions in panel D were with a 100 s wait time, a 100 cm^2/min rate, and a 10 μM pet peptoid solution.

to the equilibrium pressure, the area of the trough remains stable after an initial adjustment. At $(Nae-Npe)_{18}$ and $(Nce-Npe)_{18}$ concentrations of 10 μM each in a room-temperature, pH 9 buffer (see Experimental Section), the equilibrium pressure is 30 mN/m (see Figure 4C), and it takes 450 s for a clean interface to reach ~90% of the equilibrium pressure.

Notably, the surface area decreases exponentially with time when set to pressures above the equilibrium but below the collapse pressure. This is consistent with dissolution of the monolayer to the subphase, controlled by a desorption barrier.[24] This pathway of losing material to the subphase could also explain an inconsistency between the relatively small amounts of sheet material produced per compression cycle, compared to the total change in absolute surface area of the interface per compression. During compression there is likely a competing and perhaps predominant pathway where surface peptoids are re-dissolved into the subphase. The amount of observed macroscopic sheet material could also be due to production of sheets that are too small to be identified with the optical image analysis scheme used.

While the production of macroscopic nanosheets is strongly correlated to the emergence of buckles in the monolayer, the precise mechanism of forming sheets from a buckling monolayer can only be inferred. A likely pathway is that buckling forces the monolayer into the subphase, where there is a significant energetic benefit to bury hydrophobic residues by forming a bilayer structure.[25] Once the apposed leaflets are in

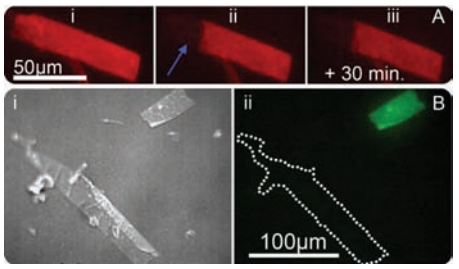

Figure 5. (A) FRAP sequence of an AlexaFluor-647-labeled nanosheet on coverslip glass (i) prior to aperture photobleaching, (ii) immediately after 30 min of photobleaching in the region labeled with a blue arrow, and (iii) 30 min later, revealing no significant change in the shape and extent of the photobleached region. (B) Covalent fluorescently labeled sheets (solvatochromic fluorophore 4-*N*,*N*-dimethylamino-1,8-naphthalimide, DMN) were dialyzed, mixed 1:4 (v/v) with unlabeled sheet-forming peptoids, and rotated in a vial ~72 times before deposition onto a 1% agarose gel. (i) Differential interference contrast bright-field image showing two adjacent sheets. (ii) Fluorescence image revealing that only one of the sheets fluoresces, indicating that little peptoid strand exchange occurs between sheets either in solution or during sheet production. An outline of the sheet in (i) is overlaid for comparison.

close proximity, short-range aromatic $\pi-\pi$ interactions[26] likely further stabilize the structure.

Implications of the Formation Mechanism. In order to convincingly demonstrate that formation of the peptoid monolayer at the air−water interface is essential for macroscopic nanosheet formation, we investigated the impact of competing surfactants on nanosheet yield. If the surfactant can inhibit sheet formation at concentrations below its critical micelle concentration (CMC), it strongly suggests that the production of macroscopic sheets occurs at the air−water interface and not in the bulk. We chose a charge neutral, zwitterionic surfactant, Zwittergent 3-12 (*n*-dodecyl-*N*,*N*-dimethyl-3-ammonio-1-propanesulfonate), to avoid unwanted electrostatic complexation with the polyionic peptoid strands. We introduced Zwittergent 3-12 over a 0−1000 μM concentration range prior to rotating the vial at 0.6 rpm for 20−26 h and monitored the yield of sheets produced by fluorescence imaging. Macroscopic sheet production began to be significantly impacted at 30 μM Zwittergent 3-12 (by 37%, 1/e). Sheet production was effectively halted at surfactant concentrations approaching 250 μM, well below the Zwittergent's measured CMC of 4 mM. This indicates that micelles trapping peptoids in the subphase is not the primary mechanism for production inhibition. Importantly, the concentration of Zwittergent that partially inhibited sheet production (30 μM) had a negligible effect on the quantity of already-formed peptoid nanosheets in solution after 24 h of exposure, indicating that the effect of the surfactant is to inhibit sheet production, not to de-stabilize already formed nanosheets. The ability of a very low surfactant concentration to inhibit sheet formation indicates that it disrupts or prevents an ordered peptoid monolayer from forming at the air−water interface, consistent with the hypothesis of sheet formation from the surface monolayer.

A key distinguishing feature of this system compared to other surfactant systems, such as phospholipids, is that the compression products are extraordinarily stable. For example, if one compresses a monolayer of phospholipids beyond the collapse pressure, the monolayer buds off vesicles[27,28] that are not stable and re-adsorb as monolayers at the air−water interface.[29] In contrast, the nanosheets do not spontaneously re-dissolve and do not exchange strands at a significant rate compared to a fluid lipid bilayer. Direct imaging of nanosheets shows little change in their morphology after several days. Additionally, monitoring the surface pressure over the course of nanosheet production also provides evidence that the process is irreversible on experimental time scales. While initially the shape of the compression isotherms is very similar from compression to compression, after a sufficient number of cycles soluble material is consumed, and the compression ratio required to reach the point of collapse increases dramatically (Figure 4D). Once the required compression ratio exceeds the capability of the Langmuir trough, then the isotherms are again comparable from compression to compression but do not exhibit a point of collapse and have significantly less hysteresis. At this stage the surface pressure after expansion is also reduced to approximately that of clean water (~0.3 mN/m). Comparing this surface pressure to the surface pressure vs concentration measurements (Figure 3A) indicates that more than 95% of the peptoids are no longer available in solution. This is consistent with free peptoids in the subphase being consumed by transformation into a more stable state than the surface monolayer.

The linear relationship between the sheet yield and the number of compressions (Figure 2B) also reveals details about the stability of nanosheets. If nanosheets nucleate additional growth in the solution, then we would observe enhanced total nanosheet areas in vials over time. Similarly, if nanosheets dissolve, we would expect depressed total sheet areas in vials over time. Since either of these effects would result in a nonlinear relationship, it is likely that both of these effects are minimal.

However, this evidence is indirect, and to preclude the possibility that both effects are acting in opposition to one another, further studies were performed. To directly test the stability of nanosheets, we performed two experiments with nanosheet analogues where 1% of the peptoids were covalently labeled with fluorescent dyes (see Experimental Section for details). First, a portion of a fluorescing nanosheet was photobleached, and it did not recover its intensity on a 1 h time scale (Figure 5A). This indicates that strands within the sheet are laterally stable and immobile. Second, the fluorescing sheets were isolated by dialysis and subsequently mixed with a non-fluorescing sheet-producing solution at a 4:1 (v/v) ratio. After further surface compressions, two distinct sheet populations, fluorescing and non-fluorescing, were observed in the subphase (Figure 5B). This indicates that the nanosheets do not nucleate their own growth in the subphase or readily fuse with neighboring sheets, suggesting the nanosheet edges are inactive. It also indicates that nanosheets do not appreciably dissolve into the monolayer at the air−water interface to form new sheets with subsequent compressions. Taken together, along with the changes in the isotherms after compressions, these observations establish the stability of the nanosheets and their inability to revert to a monolayer on experimental time scales.

Our monolayer buckling model implies that nanosheets are formed by contact between two apposed peptoid monolayers. If true, then this suggests that sheets could also be produced by direct interfacial contact. For example, in lipid systems, passing a porous hydrophobic material through the monolayer,[30] or bringing two monolayer-coated droplets into physical contact in a hydrophobic medium,[31] produces bilayers by direct interfacial

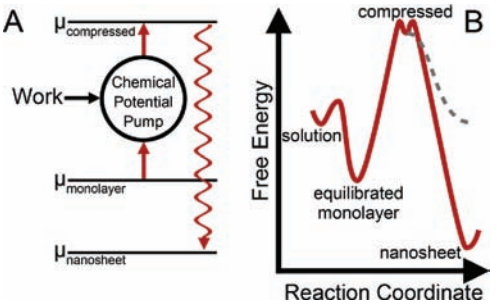

Figure 6. (A) Chemical potential pump diagram of nanosheet production from soluble peptoid by monolayer compression. (B) Relative free energy states along the physical reaction coordinate toward nanosheet formation. The dashed gray line indicates an alternate path where peptoids diffuse back into the solution.

contact. We have observed that the latter approach also produces nanosheets, although inconsistently (see SI). This is particularly relevant, as shaking a partially filled vial undoubtedly causes some interfacial contact to occur. However, while the interfacial contact approach may be useful for positioning a nanosheet in a specific geometry (e.g., over a pore), it is inadequate for large-scale nanosheet production because the approach is not readily scalable, nor does it efficiently use the available material in the subphase. The monolayer compression mechanism of making peptoid nanosheets is particularly appealing because it is scalable and able to convert as much as 95% of the material in the subphase into product.

The compression of the air−water interface is an efficient means of applying mechanical energy to the chemical potential of the peptoids (Figure 6A), likely encouraging chain alignment and increasing surface pressure until the monolayer collapses, producing nanosheets. The nanosheets are considerably more stable than the monolayer, and thus the monolayer serves as the key structural intermediate for nanosheet formation (Figure 6B). The reduced dimensionality of the monolayer significantly pre-organizes the strands favorably as compared to bulk solution.

We have previously demonstrated that the formation of peptoid nanosheets has very specific sequence requirements.[7,9] But just as in the case of protein folding, although all the structural information for the nanosheet is encoded in the monomer sequence,[32] the sequence does not always spontaneously fold into the desired thermodynamically stable structure and may require external stabilization of a structural intermediate.[33,34]

Since the air−water interface dramatically accelerates the production of nanosheets and is not consumed in the process, we can draw analogies to catalytic behavior. This is similar to the way lipid membranes have been treated as catalysts for mediating peptide−receptor interactions.[35] Like traditional catalysts, the air−water interface serves to locally orient and enrich the concentration of reactants (peptoids). Once the interface organizes the peptoids into a monolayer, applied surface compression induces collapse to form nanosheets. This pathway for nanosheet production has a dramatically lower activation energy than spontaneous assembly in the bulk (see Figure 6B). It also provides a convenient means of applying mechanical energy to overcome the activation energy. Peptoids escape the surface as nanosheets, and the air−water interface is recovered much in the way traditional catalysts are recovered after the reaction has completed. The air−water interface re-populates a monolayer of peptoids from the excess in the solution, in order to begin the next nanosheet production cycle.

CONCLUSION

Here we introduce an effective, potentially general mechanism of 2D nanomaterial synthesis by monolayer collapse. The mechanism is high yielding and cyclical, with each cycle converting soluble peptoids from solution into stable nanosheets via an intermediate monolayer at the air−water interface.

The mechanism of peptoid nanosheet production by monolayer surface compression is markedly different from using the air−water interface merely for stabilization. While copolymers,[36] lipids,[37] nanoparticles,[38] peptides,[39−42] amyloidogenic sequences,[43−45] and even macroscopic objects[46] self-assemble at various rates into defined structures at the static air−water interface, these are not structural intermediates on the way toward a lower free energy species. Peptoids form monolayers at the air−water interface (Figure 3A,C), but nanosheet production is directly correlated with compression of the monolayer beyond its collapse (Figure 2B).

We understand the relative energetics of the key intermediates (Figure 6) by comparing their relative stabilities. Nanosheets, while apparently the most stable state in the process (Figures 3B, 4D, and 5), do not form spontaneously, suggesting a large activation energy in their material synthesis. To our peptoid sequences, the air−water interface is a catalytic 2D environment that promotes lateral self-organization in the monolayer, and its compression is akin to a chemical potential pump[47] that introduces energy into the system. Once sufficient energy has been applied, the peptoid monolayer collapses into a more stable, free-floating bilayer that departs from the air−water interface.

Understanding the mechanism of nanosheet formation establishes production guidelines and design rules for functionalizing this class of 2D material. For example, encoding functional sequences that do not inhibit surface adsorption will likely retain the capacity to produce nanosheets. Furthermore, this study reveals a clean route for forming 2D nanomaterials and illustrates how interfaces must be considered to understand the complex folding rules of protein-like polymers.

EXPERIMENTAL SECTION

Peptoid Synthesis and Purification. Peptoid oligomers were synthesized on an automated robotic synthesizer using the solid-phase submonomer method[3] and purified by reverse-phase HPLC. The specifics have been described in detail elsewhere,[9] but a summary of the approach is included in the SI.

Nanosheet-Forming Solution Preparation. Aliquots of 20 μM each of $(Nae−Npe)_{18}$ and $(Nce−Npe)_{18}$ peptoids were prepared separately. $(Nae−Npe)_{18}$ was constituted in pure Milli-Q water (Millipore). $(Nce−Npe)_{18}$ was first dissolved in 40 mM NaOH at a concentration of 2 mM, and then diluted to 20 μM in 2x sheet-forming buffer: 200 mM sodium chloride, 20 mM 2-amino-2-methyl-1,3-propandiol (AMP), pH 9. The two peptoid aliquots were combined by gentle pipet aspiration.

Nanosheet Production. Nanosheets were produced from the nanosheet-forming solutions either with a Langmuir trough or by rotating vials. The Langmuir trough was commercially sourced (Mini-trough, KSV Nima, Finland), with an inverted microscopy attachment and paper Wilhelmy plates. The solutions were mixed in the trough with gentle pipet action prior to compressions. Unless otherwise noted, the wait time between compressions was typically 450 s, and the compression rate was 100 cm^2/min. To produce nanosheets by rotating

capped vials from horizontal to vertical, a device was custom-built that controlled the wait times between rotation cycles, the extent of rotation, and the rotation rate (see SI for construction details). Unless otherwise noted, nominal values were a wait time between compressions of 450 s, and a rotation angle of 85° from horizontal to vertical. A separate custom device that simply rotates the vials continuously at 0.6 rpm for 18 h was also effective at producing nanosheets. Either clean cylindrical glass vials (1 cm diameter, 3.5 cm height) or square cuvettes (1 cm^2 base, 3.5 cm height) were used, filled with equal 250 μL volumes of each peptoid-forming solution, and mixed by three gentle 250 μL pipet actions prior to rotation.

Nanosheet Fluorescence. Fluorescence imaging was performed either with covalent peptoid−fluorophore conjugates or by the addition of exogenous Nile Red, an environmentally sensitive dye whose fluorescence intensity increases substantially when it is localized in hydrophobic environments (2 μM). The incorporated fluorophores were AlexaFluor-647 (whose peptoid synthesis has been described elsewhere[9]) or a solvatochromic fluorophore, 4-*N*,*N*-dimethylamino-1,8-naphthalimide[48,49] (DMN, see SI for the chemical structure).

Nanosheet Counting. Quantitative sheet-counting was performed by depositing a known volume (e.g., 10 μL) of nanosheet solution onto pre-cleaned microscope slides, sandwiching under a coverslip of known area (e.g., 22 × 22 mm), and imaging at five random locations under epifluorescence illumination with an Olympus IX81 inverted microscope, fitted with a Hamamatsu Orca CCD camera. Statistics on sheets were gathered from these five images using custom Matlab (Mathworks, Natick, MA) scripts (see SI).

Dialysis. Sheet solutions were dialyzed using a FloatAlyzer membrane with a molecular weight cutoff of 100 kDa. Dialysis was performed overnight against a solution of 100 mM NaCl, 10 mM Tris, pH 9.0, to remove free peptoid strands.

Monolayer Imaging. Brewster angle microscopy (KSC Nima MicroBAM, Finland), bright-field imaging, and fluorescence were performed on the air−water interface of a Langmuir trough. Bright-field imaging and fluorescence were performed using the microscopy instrument described in the "nanosheet counting" section above.

Surface Tension Determination by Capillary Rise. Surface tension was measured by capillary rise using a custom-built device. The device consists of a fixed horizontal camera, lens, and light source and a vertical translation stage that holds the sample and the capillary. Glass capillaries of known inner diameters were ambient-air plasma-etched (3 min, Harrick, Ithaca, NY), and one end was dipped into freshly mixed solution (within 1 min of mixing). The base liquid level was determined by aligning it to a mark in the middle of the camera's field of view. The capillary rise was measured by the amount of vertical translation necessary to place the meniscus inside the capillary on the same mark in the camera's field of view. The surface tension was calculated with the formula $\gamma = \rho grh/(2\cos\theta)$,[21] where γ is surface tension, ρ is the density of the liquid, g is the acceleration due to gravity, r is the inner radius of the capillary, h is the measured height of the capillary action, and θ is the contact angle of the solution on glass (measured to be <5°; $\cos\theta$ is approximated as 1).

■ ASSOCIATED CONTENT

Supporting Information. Qualitative comparison of nanosheet production as a function of agitation method, movies of free-floating nanosheets in solution, calculation of the surface area of a partially filled cuvette during rotation, AFM analysis of nanosheet and monolayer heights, powder X-ray diffraction analysis, nanosheet counting software method, peptoid concentration effects, Zwittergent 3-12 inhibition of nanosheet production, surface pressure as a function of number of compressions, nanosheet formation by interfacial contact, method for peptoid synthesis, conjugated solvatochromatic dye structure, and details of vial rocking apparatus. This material is available free of charge via the Internet at http://pubs.acs.org.

■ AUTHOR INFORMATION

Corresponding Author
rnzuckermann@lbl.gov

■ ACKNOWLEDGMENT

The authors thank Stephen Whitelam, Behzad Rad, Jeremy Schmit, Ki Tae Nam, Michael D. Connolly, Bastian Barton, Carlos Olguin/Autodesk, and Promita Chakraborty for insightful discussions and valuable assistance. This work was carried out at the Molecular Foundry with support from the Advanced Light Source, at Lawrence Berkeley National Laboratory, both of which are supported by the Office of Science, Office of Basic Energy Sciences, U.S. Department of Energy, under Contract No. DE-AC02-05CH11231. The work was also funded by the Defense Threat Reduction Agency under Contract No. IACRO-B0845281.

■ REFERENCES

(1) Hawker, C.; Wooley, K. *Science* **2005**, *309*, 1200.
(2) Goodman, C.; Choi, S.; Shandler, S.; DeGrado, W. *Nat. Chem. Biol.* **2007**, *3*, 252.
(3) Zuckermann, R.; Kerr, J.; Kent, S.; Moos, W. *J. Am. Chem. Soc.* **1992**, *114*, 10646.
(4) Simon, R.; Kania, R.; Zuckermann, R.; Huebner, V.; Jewell, D.; Banville, S.; Ng, S.; Wang, L.; Rosenberg, S.; Marlowe, C. *Proc. Natl. Acad. Sci. U. S. A.* **1992**, *89*, 9367.
(5) Burkoth, T.; Beausoleil, E.; Kaur, S.; Tang, D.; Cohen, F.; Zuckermann, R. *Chem. Biol.* **2002**, *9*, 647.
(6) Miller, S. M.; Simon, R. J.; Ng, S.; Zuckermann, R. N.; Kerr, J. M.; Moos, W. H. *Bioorg. Med. Chem. Lett.* **1994**, *4*, 2657.
(7) Kudirka, R.; Tran, H.; Sanii, B.; Nam, K. T.; Choi, P. H.; Venkateswaran, N.; Chen, R.; Whitelam, S.; Zuckermann, R. N. *Biopolymers* **2011**, *96*, 586.
(8) Murnen, H.; Rosales, A.; Jaworski, J.; Segalman, R.; Zuckermann, R. *J. Am. Chem. Soc.* **2010**, 55.
(9) Nam, K. T.; Shelby, S. A.; Choi, P. H.; Marciel, A. B.; Chen, R.; Tan, L.; Chu, T. K.; Mesch, R. A.; Lee, B. C.; Connolly, M. D.; Kisielowski, C.; Zuckermann, R. N. *Nat. Mater.* **2010**, *9*, 454.
(10) Sakamoto, J.; van Heijst, J.; Lukin, O.; Schlüter, A. D. *Angew. Chem., Int. Ed.* **2009**, *48*, 1030.
(11) Nottbohm, C. T.; Turchanin, A.; Beyer, A.; Stosch, R.; Gölzhäuser, A. *Small* **2011**, *7*, 874.
(12) Peng, C.; Jiang, B.; Liu, Q.; Guo, Z.; Xu, Z.; Huang, Q.; Xu, H.; Tai, R.; Fan, C. *Energy Environ. Sci.* **2011**, *4*, 2035.
(13) Tang, Z.; Zhang, Z.; Wang, Y.; Glotzer, S. C.; Kotov, N. A. *Science* **2006**, *314*, 274.
(14) Grzybowski, B. A.; Wilmer, C. E.; Kim, J.; Browne, K. P.; Bishop, K. J. M. *Soft Matter* **2009**, *5*, 1110.
(15) Whitesides, G. M. *Small* **2005**, *1*, 172.
(16) Ariga, K.; Hill, J. P.; Lee, M. V.; Vinu, A.; Charvet, R.; Acharya, S. *Sci. Technol. Adv. Mater.* **2008**, *9*, 014109.
(17) Brack, A.; Caille, A. *Int. J. Pept. Protein Res.* **1978**, *11*, 128.
(18) Chi, E. Y.; Frey, S. L.; Winans, A.; Lam, K. L. H.; Kjaer, K.; Majewski, J.; Lee, K. Y. C. *Biophys. J.* **2010**, *98*, 2299.
(19) Gaines, G. L. *Insoluble monolayers at liquid-gas interfaces*; Interscience Publishers: New York, 1966.
(20) Hauksbee, F. *Philos. Trans.* **1712**, *28*, 151.
(21) de Gennes, P. G. *Rev. Mod. Phys.* **1985**, *57*, 827.
(22) Hoenig, D.; Moebius, D. *J. Phys. Chem.* **1991**, *95*, 4590.

(23) Jiang, D.; Dinh, K. L.; Ruthenburg, T. C.; Zhang, Y.; Su, L.; Land, D. P.; Zhou, F. *J. Phys. Chem. B* **2009**, *113*, 3160.
(24) Smith, R. D.; Berg, J. C. *J. Colloid Interface Sci.* **1980**, *74*, 273.
(25) Lu, W.; Knobler, C. M.; Bruinsma, R. F.; Twardos, M.; Dennin, M. *Phys. Rev. Lett.* **2002**, *89*, 146107.
(26) Sato, T.; Tsuneda, T.; Hirao, K. *J. Chem. Phys.* **2005**, *123*, 104307.
(27) Gopal, A.; Lee, K. Y. C. *J. Phys. Chem. B* **2001**, *105*, 10348.
(28) Wiese, W.; Harbich, W.; Helfrich, W. *J. Phys: CM* **1992**, *4*, 1647.
(29) Tajima, K.; Gershfeld, N. *Biophys. J.* **1985**, *47*, 203.
(30) Montal, M.; Mueller, P. *Proc. Natl. Acad. Sci. U.S.A.* **1972**, *69*, 3561.
(31) Holden, M. A.; Needham, D.; Bayley, H. *J. Am. Chem. Soc.* **2007**, *129*, 8650.
(32) Anfinsen, C. *Science* **1973**, *181*, 223.
(33) Sigler, P.; Xu, Z.; Rye, H.; Burston, S.; Fenton, W.; Horwich, A. *Annu. Rev. Biochem.* **1998**, *67*, 581.
(34) Dill, K.; Chan, H. *Nat. Struct. Biol.* **1997**, *4*, 10.
(35) Sargent, D.; Schwyzer, R. *Proc. Natl. Acad. Sci. U.S.A.* **1986**, *83*, 5774.
(36) Cox, J.; Yu, K.; Constantine, B.; Eisenberg, A.; Lennox, R. *Langmuir* **1999**, *15*, 7714.
(37) McConnell, H. *Annu. Rev. Phys. Chem.* **1991**, *42*, 171.
(38) Boker, A.; He, J.; Emrick, T.; Russell, T. P. *Soft Matter* **2007**, *3*, 1231.
(39) Chen, H.; Hsu, S. L.; Tirrell, D. A.; Stidham, H. D. *Langmuir* **1997**, *13*, 4775.
(40) Malcolm, B. R. *J. Colloid Interface Sci.* **1985**, *104*, 520.
(41) Rapaport, H.; Kjaer, K.; Jensen, T. R.; Leiserowitz, L.; Tirrell, D. A. *J. Am. Chem. Soc.* **2000**, *122*, 12523.
(42) Taylor, J. *Adv. Space Res.* **1986**, *6*, 19.
(43) Lepère, M.; Chevallard, C.; Hernandez, J.; Mitraki, A.; Guenoun, P. *Langmuir* **2007**, *23*, 8150.
(44) Pronchik, J.; He, X.; Giurleo, J. T.; Talaga, D. S. *J. Am. Chem. Soc.* **2010**, *132*, 9797.
(45) Schladitz, C.; Vieira, E.; Hermel, H.; Möhwald, H. *Biophys. J.* **1999**, *77*, 3305.
(46) Bowden, N.; Terfort, A.; Carbeck, J.; Whitesides, G. *Science* **1997**, *276*, 233.
(47) Hoffmann, K. H.; Burzler, J. M.; Schubert, S. *J. Non-Equil. Therm.* **1997**, *22*, 311.
(48) Loving, G.; Imperiali, B. *J. Am. Chem. Soc.* **2008**, *130*, 13630.
(49) Wu, A.; Xu, Y.; Qian, X. *Monatsh. Chem.* **2010**, *141*, 893.